Nickel Complexes for Robust Light-Driven and Electrocatalytic Hydrogen Production from Water

ARTICLE *in* ACS CATALYSIS · JANUARY 2015

Impact Factor: 9.31 · DOI: 10.1021/acscatal.5b00045

5 AUTHORS, INCLUDING:

Amit Das
University of Wisconsin–Madison
15 PUBLICATIONS **186** CITATIONS

ACS Catalysis

Research Article

pubs.acs.org/acscatalysis

Nickel Complexes for Robust Light-Driven and Electrocatalytic Hydrogen Production from Water

Amit Das,[†,#] Zhiji Han,[†,#] William W. Brennessel,[†] Patrick L. Holland,[‡] and Richard Eisenberg*[,†]

[†]Department of Chemistry, University of Rochester, RC Box 270216, Rochester, New York 14627, United States

[‡]Department of Chemistry, Yale University, P.O. Box 208107, New Haven, Connecticut 06511, United States

Supporting Information

ABSTRACT: A series of nickel bis(chelate) complexes having square planar coordination are studied for light-driven and electrocatalytic hydrogen production from water. The complexes $Ni(abt)_2$ (abt = 2-aminobenzenethiolate), $Ni(mp)_2$ (mp = 2-mercaptophenolate) and $Ni(mpo)_2$ (mpo = 2-mercaptopyridyl-*N*-oxide) are found to be active catalysts under light-driven conditions, using fluorescein (Fl) as the photosensitizer (PS) and triethanolamine (TEOA) as the sacrificial electron donor in water under basic pH (pH = 9.8). These molecular systems achieve a turnover number (TON) of ~6000 (relative to catalyst) and are stable for more than 100 h under H_2-generating conditions. When water-soluble CdSe quantum dots with tripodal S-donor capping agents are employed as PS and ascorbic acid (AA) is used as the sacrificial electron donor at pH 4.5, an active and robust system is obtained for the light-driven generation of H_2 from aqueous protons. A TON of over 280 000 is achieved for the three active catalysts. These complexes are also examined electrochemically in organic solvents with weak organic acids as the proton source and in aqueous and aqueous/organic media for proton reduction. The most active photochemical catalysts also show excellent electrocatalytic activity in neutral pH water, achieving Faradaic yields close to 100% under anaerobic conditions and ~80% under aerobic conditions.

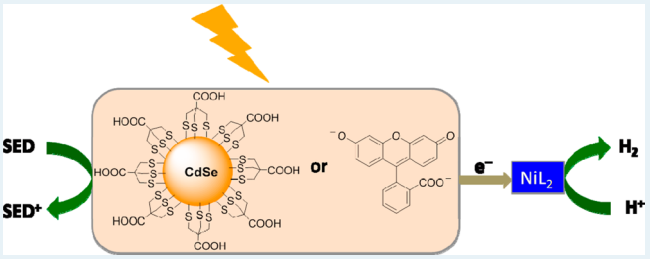

KEYWORDS: *photochemistry, hydrogen evolution, molecular HER catalysis, Ni catalysts with redox active ligands, CdSe quantum dots, HER mechanism, fluorescein, heterocoupling*

INTRODUCTION

The projected worldwide demand for energy[1] requires that sources of alternative energy increase rapidly in order to reduce (and eventually reverse) the growth of CO_2 emissions and its consequent effects on global climate change. Over 80% of the world's energy consumption originates from carbon-based fossil fuels, which has led to an increase in atmospheric CO_2 from 315 ppm in 1957 to 400 ppm in 2013 with projections in the range of 490−570 ppm by 2050.[1−3] The most viable path for large-scale growth in carbon-free energy involves solar energy conversion, and specifically the light-driven splitting of water into its constituent elements.[4−6] Water splitting is a redox reaction in which aqueous protons are reduced into H_2 and water is oxidized to O_2. Both light-driven artificial photosynthesis (AP) and electrochemical systems for hydrogen generation from water have been investigated extensively.[7−14] Here, we report a study on the proton reduction side of water splitting, examining this half-reaction in the absence of other important parts of a complete AP system.

Within the past decade, there has been significant and accelerating progress in developing first-row transition metal catalysts in place of rare noble metal catalysts for proton reduction to hydrogen.[15−22] Robustness, activity, and functionality under a variety of conditions of first-row transition metal catalysts for the light-driven generation of hydrogen remain a challenge. For example, tetraazamacrocycle cobalt complexes have been reported to be active electrocatalysts for proton reduction in acidic water with Faradaic efficiencies up to 92% and overpotentials (η) of ~650 mV,[11] but these catalysts achieve less than 400 turnovers (TON) of H_2 in a variety of light-driven AP systems,[23−28] possibly due to photodecomposition and ligand hydrogenation.[26,29,30] In other examples, Mo and Co polypyridyl complexes have been reported to exhibit great electrocatalytic activities in neutral or slightly acidic water with an overpotential of >400 mV,[31−33] but the TONs of the Co complexes in light-driven AP systems (up to 1630 TON) are much lower than those in the electrocatalytic systems (>50 000 TON).[33,34] In yet another example, Ni bis(diphosphine) complexes have been found to promote turnover frequencies (TOF) of ~100 000 s^{-1} for electrocatalytic proton reduction in organic or mixed organic/aqueous solvents,[12,35,36] but the use of one of these complexes in a light-driven AP system shows only a low TOF of 20 h^{-1} with molecular photosensitizers (PS) at pH 2.[37] Though a higher TOF can be obtained when binding the catalyst to the Photosystem I protein, the overall TON of the system does not improve.[38]

Received: January 11, 2015

DOI: 10.1021/acscatal.5b00045
ACS Catal. 2015, 5, 1397−1406

In our laboratory, significant progress has been made recently in finding and analyzing highly active molecular catalysts for light-driven systems to produce H_2.[17,18,39,40] One set of catalysts consists of bis(benzenedithiolate) (bdt) complexes of cobalt. Benzene-1,2-dithiolate is a dithiolene that is known to be redox active when coordinated. Complexes of dithiolenes, which have been studied for decades,[41−43] exhibit redox processes that may occur on the ligand as well as the metal, making such systems potential reservoirs of charge in multielectron processes.[44] Additionally, ligand sites corresponding to S and N donors are available for protonation, thus allowing these systems the ability to assemble the two protons and two electrons to make H_2 from stepwise electron-transfers and protonations. Computational studies by Solis and Hammes-Schiffer support this idea with results that are consistent with electron addition into an orbital of mixed metal and ligand character and protonation at a dithiolene S donor atom.[45] Although the Co bis(dithiolene) catalysts were initially employed for light-driven H_2 generation with Ru(bpy)$_3^{2+}$ as the photoactive element,[17,46] more recent work has involved their use in aqueous systems with CdSe quantum dot (QD) light absorbers having water-solubilizing, exchange-inert tridentate S-donor capping agents.[47] Other recent studies from our laboratory have involved Ni pyridinethiolate (pyS) and pyrimidinethiolate complexes as hydrogen-generating catalysts with fluorescein (Fl) as the PS.[18,39] With these catalysts, dechelation and protonation of a pyridyl (or pyrimidinyl) N donor were proposed as integral parts of the mechanism for H_2 formation.

In the present study, square planar nickel complexes **1**−**4** (Scheme 1) having other redox noninnocent ligands are

Scheme 1. Molecular Structures of the Catalysts

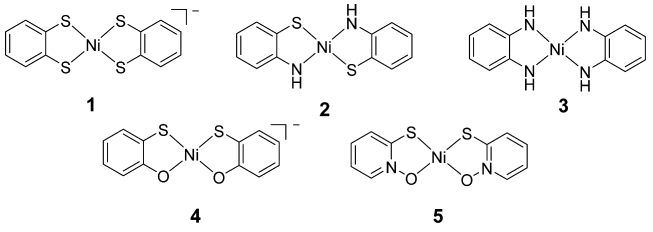

examined regarding their catalytic behavior for hydrogen generation in both basic and acidic systems with either Fl or CdSe QDs as light absorbers. Bis(chelate) complexes **1**−**4** contain bdt or analogues having S, O, or NH as donors for coordination to the Ni centers. Also examined is complex **5** (Scheme 1) that contains a structurally similar 2-pyridinethiolate-*N*-oxide chelating ligand. We find that three of the complexes exhibit high levels of activity and durability with both Fl and CdSe QDs photosensitizers for proton reduction to give H_2. Additionally, stoichiometric experiments show that the reduction of protons to H_2 by **2** proceeds through the anion of complex **6**, which supports a heterocoupling mechanism for hydrogen generation.

RESULTS AND DISCUSSION

Synthesis and Characterization. Complexes **1**−**5** were synthesized following literature procedures, with a minor modification of the method of crystallization for **5** (see Experimental Section).[48−53] The purities of the samples were confirmed by elemental analyses, which match well with theoretically calculated values (see Experimental Section). Among the five complexes, **2**, **3**, and **5** are obtained in their neutral forms, whereas complexes **1** and **4** are isolated as monoanions with tetrabutylammonium as the countercation. ^{1}H NMR spectra of **2**, **3**, and **5** exhibit sharp signals within the chemical shift range of δ 0−10 ppm (see Experimental section and Figures S2, S3, and S5), indicating a diamagnetic ground state for these complexes. In contrast, the monoanionic complexes **1** and **4** have been reported to be paramagnetic[48,49,54] and are found to exhibit no sharp ^{1}H NMR resonances for their respective phenyl protons, Figures S1 and S4.

The electronic spectra of complexes **1**−**5** are shown in Figure 1 with absorption maxima and molar absorptivities given in

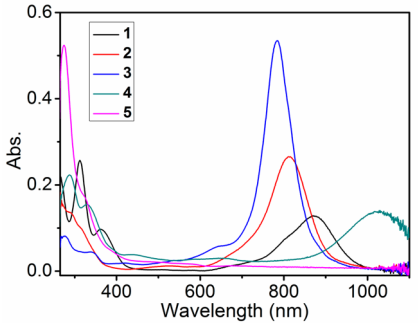

Figure 1. UV−vis-NIR absorption spectra of complexes **1**−**5** (10^{-5} M) in DMF.

Table S1. Complexes **1**−**4** exhibit strong absorption bands in the 800−1100 nm region of the spectrum that have been characterized previously[55] as ligand-to-ligand charge transfer (LLCT) bands resulting from the fact that at least one of the ligands has a monoanionic formulation and radical character. Complex **5** has no such LLCT band, indicating that the mpo ligand with a pyridine *N*-oxide donor is *not* redox active despite its structural similarity to the other thiolate complexes. Neutral complexes **2** and **3** contain two radical ligands with the nickel ion present in its +2 oxidation state and d^8 electron configuration.[55,56] Monoanionic complexes **1** and **4** each have one radical ligand with the LLCT transition occurring at lower energy than those for **2** or **3**. For the monoanionic complexes, the ground state configuration can best be formulated as $[Ni^{II}(L^{\bullet-})(L^{2-})]^-$, although the anisotropic nature of their EPR spectra does not rule out the alternative formulation of $[Ni^{III}(L^{2-})]^-$.[49,54]

Structures of the Complexes. Complexes **1**−**5** all have square planar coordination. However, because of the asymmetry of chelating ligands with different donor atoms, complexes **2**, **4**, and **5** can have either *cis* or *trans* arrangements. The previously reported crystal structures of complexes **4** and **5** show only the *cis* configuration.[51,57] A related Pd(mpo)$_2$ complex also exhibits a *cis* arrangement in the crystal structure.[58] However, Zn(4-Me-mpo)$_2$ (4-Me-mpo = 4-methyl-2-mercaptopyridyl *N*-oxide) has been reported to adopt a *trans* arrangement in its solid state structure.[59] While the *cis* or *trans* ligand arrangement of complex **5** *in solution* has not been identified, its ^{1}H NMR spectrum shows only four sharp resonances of the aromatic protons (Figure S5).

The crystal structure of **2** (Figure 2A) shows the presence of the N-deprotonated *ortho*-aminobenzenethiolate ligands in a *trans* arrangement around the square planar coordinated Ni^{2+}

DOI: 10.1021/acscatal.5b00045
ACS Catal. 2015, 5, 1397−1406

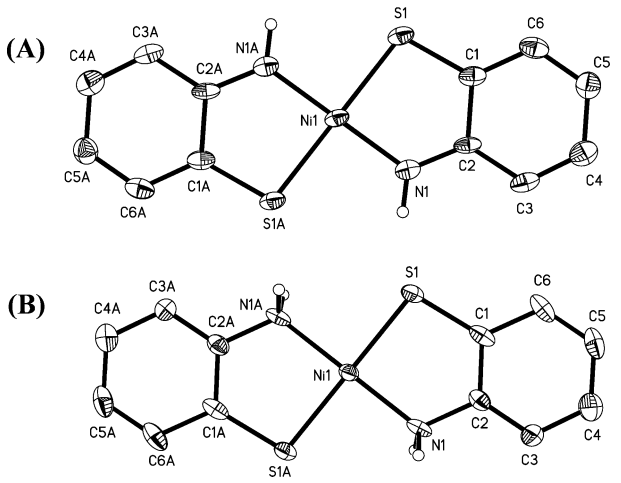

Figure 2. ORTEP diagrams of (A) **2** and (B) **6**. The ellipsoids are drawn at the 50% probability level. All the hydrogen atoms except the ones bound to nitrogen have been omitted for clarity.

ion. The C(2)−N(1) and C(1)−S(1) bond distances are 1.343(7) and 1.706(6) Å, respectively, and the C−C distances exhibit a long−short alternation that is consistent with previously reported semi(imino)thioquinone ligands.[60] The structural results are thus in accord with the view of **2** as a nickel(II) complex with antiferromagnetically coupled radical ligands. The ^{1}H NMR spectrum of the complex shows four signals for the aromatic protons, indicating the presence of only one isomer in solution (see Experimental Section and Figure S2).

Complex **2** can be converted by the addition of 2 H^+ and 2 e^- to complex **6** which has also been characterized crystallographically (see Figure 2B). Complex **6** is formally a classical complex with each *o*-aminobenzenethiolate ligand having a charge of 1− and all electrons paired. The structure of complex **6** is shown in Figure 2B, and all metrical parameters are provided in Supporting Information. As expected, the respective C(2)−N(1) and C(1)−S(1) bond distances of 1.435(6) and 1.762(5) Å are longer than the corresponding distances (1.343(7) and 1.706(6) Å, respectively) in **2** and match well with the aminothiolato C−N and C−S bond distances reported in the literature.[60] Within the errors of the structure determination, the structure of **6** is consistent with a fully delocalized aromatic ring. Complex **6** does not show any strong absorption in the 800−1000 nm region of the spectrum (Figure S7), consistent with the classical, diamagnetic nature of its ligands.

The conversion of **2** to **6** was carried out by the addition of acetic acid to a 1×10^{-5} M solution of **2** in dimethylformamide (DMF) followed by the addition of decamethylcobaltocene ($Co(Cp^*)_2$) as a reducing agent (Figure S6). The conversion is reversible by the treatment of **6** with base (NEt_3) followed by the addition of ferrocenium tetrafluoroborate ($FcBF_4$) as oxidizing agent. Figures 3 and S7 follow the conversion of **6** to **2** with isosbestic points noted at 332 and 275 nm. The results indicate that any intermediates formed in the interconversion of these two complexes (Scheme 2), which is solely ligand-based, are present in negligible amounts.

Light-Driven Hydrogen Production. The hydrogen-generating abilities of complexes **1**−**5** were studied under photochemical conditions using initially the organic dye Fl as the PS, and subsequently exchange-inert CdSe QDs as the PS.

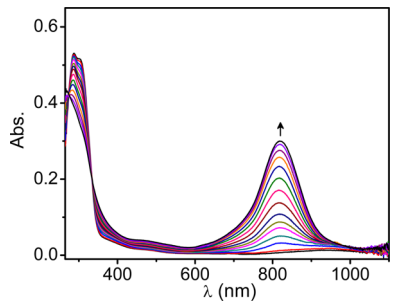

Figure 3. UV−vis spectral change upon titration of ferrocenium tetrafluoroborate to a solution containing **6** (1×10^{-5} M) and 2 equiv of triethylamine in DMF. For triethylamine addition to **6**, see Figure S7.

Scheme 2. Chemical Interconversion of 6 and 2 with 2 Drawn To Indicate the Ligand Radical Character

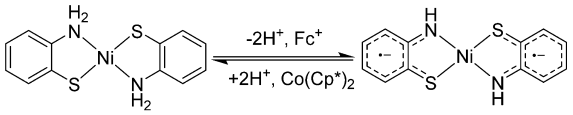

6 **2**

The capping agent that makes the CdSe QDs inert to ligand exchange is 3-thio-2,2-di(mercaptomethyl)propionate ($^-SCH_2)_3CCOO^-$, denoted S3). Both sets of experiments were conducted in aqueous solutions and required the addition of a sacrificial electron donor (SED) that differed between the two sets of experiments. When Fl was the PS, triethanolamine (TEOA) served as the electron donor and the sample pH was 9.8, whereas when the S3-capped-CdSe QDs were employed as PS, ascorbic acid (AA) functioned as the electron source, and the sample pH was 4.5. The light source was a green light emitting diode (λ = 520 nm, 13 mW/cm^2). The pressure change in the sample headspace was followed during irradiation, and the amount of H_2 produced was quantified by gas chromatographic (GC) analysis in which a fixed amount of methane was added *prior* to irradiation as an internal standard for the GC analysis.

For the series of experiments using Fl as PS (Figure 4), catalysts **2**, **4**, and **5** exhibited similar activity in terms of total turnover numbers (TONs) (~6000 mol of H_2 per mole of catalyst in 100 h), whereas the TON for the sample using complex **3** was much lower (~900). Under these conditions,

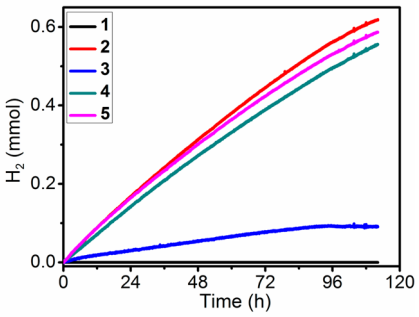

Figure 4. Light-driven hydrogen production from a system containing Fl (2.0 mM) and TEOA (0.35 M) in H_2O (5.0 mL) at pH 9.8 with different nickel catalysts at 20.0 μM **1** (black), **2** (red), **3** (blue), **4** (cyan), and **5** (pink) upon irradiation with 520 nm LED (13 mW/cm^2) at 15 °C.

DOI: 10.1021/acscatal.5b00045
ACS Catal. 2015, 5, 1397−1406

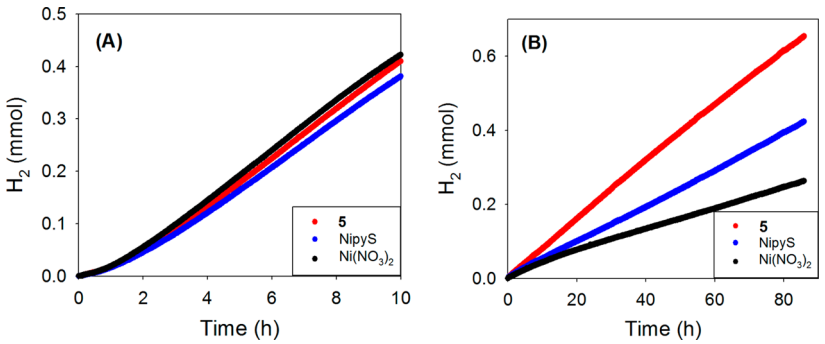

Figure 5. Light-driven hydrogen production from a system containing (A) DHLA-CdSe QDs (530 nm) (4.0 μM) and AA (0.5 M) in H_2O (5.0 mL) at pH 4.5 with different nickel catalysts at 1.0 μM **5** (red), $Ni(pyS)_3^-$ (blue), $Ni(NO_3)_2$ (black). (B) S3-CdSe QDs (530 nm) (2.0 μM) and AA (0.5 M) in H_2O (5.0 mL) at pH 4.5 with different nickel catalysts at 1.0 μM **5** (red), $Ni(pyS)_3^-$ (blue), and $Ni(NO_3)_2$ (black), upon irradiation with 520 nm LED (13 mW/cm^2) at 15 °C.

complex **1** was observed to be inactive for H_2 generation in marked contrast with its Co analogue, $Co(bdt)_2^-$, which had been reported previously to be both active and durable for H_2 production, albeit with a different molecular PS.[17,46]

UV−vis spectra collected during the photocatalytic experiments reveal that Fl decomposition, which occurs within 5 min in the presence of TEOA alone, happens much more slowly when catalyst is present along with TEOA, showing 26% of Fl still left in solution after 90 h of irradiation (Figure S9). Similar results have been reported previously using pyridylthiolate complexes of Ni^{2+} and are consistent with reductive quenching of Fl followed by a unimolecular decomposition of Fl^- that is slow relative to bimolecular electron-transfer between Fl^- and the catalyst.[39] A Hg-poisoning test was used to determine if colloidal Ni (potentially formed during irradiation) functions as the catalyst in the system containing **2** (Figure S10).[16] Addition of Hg to the photochemical system does *not* alter the initial rate of hydrogen production, and the system possesses similar activity to what was observed when no Hg is added. This experiment supports the homogeneous nature of the Fl/catalyst/TEOA system for light-driven H_2 generation. Another control experiment was conducted in which $Ni(NO_3)_2$ was used in place of **2** for photochemical H_2 production. This system generates negligible amounts of hydrogen relative to the system using **2** as the catalyst (Figure S11).

The activity of complexes **1**−**5** as catalysts in the photogeneration of hydrogen was subsequently examined in systems using water-soluble CdSe QDs as the PS and ascorbic acid (AA) as the electron donor at pH 4.5. The QDs were synthesized following reported methods and made water-soluble using the S3 capping agent.[20,47] For examination of catalyst activity, the S3-capped CdSe QDs offer a great advantage over CdSe QDs capped by mono- or bidentate ligands because the resultant QDs do not dissociate the capping agent, which can coordinate to the catalyst, as illustrated by the following example.[47] When CdSe QDs capped with dihydrolipoic acid (DHLA) anion were used with complex **5**, the system exhibited the same level of activity as when $Ni(NO_3)_2$ or $Ni(pyS)_3^-$ were used as the catalyst, consistent with $Ni(DHLA)_x$ formation in situ[20] (Figure 5A), whereas when the S3 capped-CdSe QDs were employed (specific concentrations: 2.0 μM [S3-CdSe QDs], 1.0 μM [catalyst], 0.5 M [AA]), both TOF and TON values were found to increase in the order $Ni(NO_3)_2$ < $Ni(pyS)_3^-$< **5** (Figure 5B). The system containing **5** as the catalyst is robust with no degradation observed over a 90 h period under irradiation, a TOF of 1550 mol of H_2 per hour (relative to catalyst) and a total TON of >130 000 for this period.

The Ni complexes **1**−**5** were compared directly under slightly different conditions as shown in Figure 6. Complexes **2**, **4**, and **5** exhibit the highest activities with >280 000 TON in 1 week, whereas systems with complexes **1** and **3** show distinctly poorer results in terms of light-driven H_2 generation. The general order of catalytic activity for the five complexes was the same as for the corresponding homogeneous systems employing Fl as the PS with TEOA as the sacrificial donor. The reasons for the similarity in order of activity are not immediately apparent because the systems containing Fl function by *reductive* quenching of Fl* to yield Fl^- followed by electron transfer to the catalyst at pH 9.8,[18] whereas the systems containing the S3 capped-CdSe QDs proceed by electron-transfer *from* the excited QD to the catalyst at pH 4.5.[20]

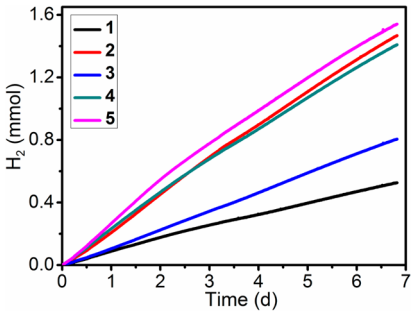

Figure 6. Light-driven hydrogen production from a system containing S3-CdSe NCs (518 nm) (4.0 μM) and AA (0.5 M) in H_2O (5.0 mL) at pH 4.5 with different nickel catalysts at 1.0 μM **1** (black), **2** (red), **3** (blue), **4** (cyan), and **5** (pink) upon irradiation with 520 nm LED (13 mW/cm^2) at 15 °C and 1 atm initial pressure of N_2/CH_4 (79:21 mol %) with CH_4 as an internal standard for H_2 quantification by GC analysis.

Electrocatalytic Studies on Nickel Complexes and Correlation with Light-Driven Systems Using Fluoroscein. Our previous studies have shown that the main role of the PS is to transfer electrons to the catalyst, but this necessarily occurs at a fixed potential and is accompanied by possible changes of the catalyst from irradiation or exposure to the PS. Therefore, we pursued electrochemical experiments in order to examine the catalysts **1**−**5** under simpler conditions where the chemical potential of the reducing electrons could be varied.

DOI: 10.1021/acscatal.5b00045
ACS Catal. 2015, 5, 1397−1406

Table 1. Comparison Data for the Catalysts

complexes	E_{red1} [a]	E_{red2} [a]	E_{cat} [a]	TON_{Fl} [b]	$TON_{S3\text{-}QD}$ [c]	TOF_{Fl} [d] (h^{-1})	$TOF_{S3\text{-}QD}$ [d] (h^{-1})
1	−0.56	-	−2.25	0	105 300	0	730
2	−0.11	−0.94	−1.64	6190	293 400	75	1880
3	−0.89	−1.53	−2.03	900	161 000	16	930
4	−0.45	-	−1.62	5600	281 000	60	1940
5	−1.32	-	−1.63	5900	308 000	74	2280

[a]Potentials are in V vs SCE. Electrochemical studies were performed in MeCN (for **4** in DMF) with 0.5 mM catalyst and 0.1 M $TBAPF_6$ as supporting electrolyte. Acetic acid was used in the electrocatalytic experiments and E_{cat} was calculated at 8.0 mM acetic acid concentration. [b]TON_{Fl} = turnover number using fluorescein as PS. Experimental condition: Fl (2.0 mM), catalyst (20 μM) and TEOA (0.35 M) in H_2O (5.0 mL) at pH 9.8; temp: 15 °C. [c]$TON_{S3\text{-}QD}$ = turnover number using S3-QD as PS. Experimental condition: S3-QD (4.0 μM), catalyst (1.0 μM) and AA (0.5 M) in H_2O (5.0 mL) at pH 4.5; temp: 15 °C. [d]For Fl as PS, TOF for initial 10 h and for S3-QD as PS, TOF for initial 40 h are given.

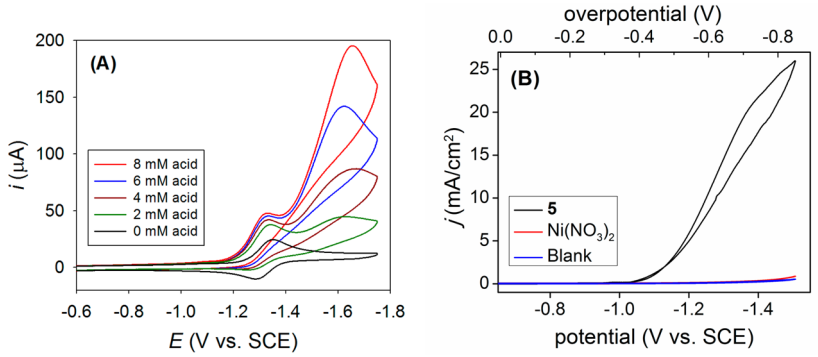

Figure 7. (A) Cyclic voltammograms of **5** (0.5 mM) in MeCN without the presence of acid (black) and in the presence of acetic acid with increasing concentration (other colors). Conditions: 0.1 M $TBAPF_6$, glassy carbon as both working and counter electrodes, scan rate 250 mV/s. (B) Cyclic voltammograms of **5** (0.1 mM) (blue) and $Ni(NO_3)_2$ (0.1 mM) (red), and a control in the absence of catalyst (black). Conditions: 1.0 M phosphate buffer at pH 7.0 under Ar, glassy carbon (0.071 cm^2) as both working and counter electrodes, SCE as the reference electrode, scan rate 100 mV/s. Overpotential = applied potential − E (pH 7).

Cyclic voltammetry (CV) experiments were conducted in dry acetonitrile or dry DMF solution depending on the solubility of the complexes (all potentials are given relative to SCE). In the absence of acid, both monoanionic complexes **1** and **4** exhibit only one reversible redox couple at −0.56 and −0.45 V respectively (Figure S12 and S15, Table 1). These are attributed to the NiL_2^{-}/NiL_2^{2-} ligand-based reductions, because the monoanionic complexes **1** and **4** each possess one radical anion ligand that is reduced to the dianion in this process.[43] The neutral complexes **2** and **3** each exhibit two reversible reduction events at −0.11 V and −0.94 V for **2**, and at −0.89 V and −1.53 V for **3** (Figure S13 and S14, Table 1). In each of these complexes, both chelating ligands are present as radical anions as determined by Wieghardt and co-workers through experimental observations and theoretical calculations.[55,56] The two reductions seen for **2** and **3** correspond to electron addition to the two half-occupied, mainly ligand-based molecular orbitals for each complex. The less negative values for the reductions of **2** relative to **3** are consistent with the presence of S in the ligand structure of **2** but not in **3**. In contrast to the results for **2** and **3**, complex **5** exhibits a single reversible reduction at −1.32 V that is attributed to the Ni^{2+}/Ni^{+} couple (Figure 7A). The lack of a second wave supports our contention that the mpo ligand is not redox active in this system.

In measurements to examine the electrocatalytic activities of **1**−**5** for H_2 production, CV responses of the complexes were measured in acetonitrile as a function of acetic acid as a possible proton source. Upon increasing additions of acetic acid to these solutions, catalytic waves are observed. These waves occur at more negative potentials than the reversible couples described above (Figure 7A and S11−14) with the latter becoming irreversible. The results indicate that the initial reduction of the complex is not the turnover limiting step, as discussed below.

The catalytic wave for **1**, which is minimally active as a catalyst for light-driven H_2 generation, occurs at −2.25 V in acetonitrile. This value is much more negative than the reduction potential of the reduced Fl (−1.3 V), which suggests that electron-transfer from Fl^{-} to **1** is not feasible, thus explaining why the Fl/**1**/TEOA system is ineffective for H_2 generation. Likewise, complex **3** exhibits a catalytic wave at ca. −2.03 V and therefore exhibits poor activity for H_2 generation as a consequence of the unfavorable electron transfer step from Fl^{-} to the catalyst. In contrast, the three most active catalysts for light-driven H_2 generation (**2**, **4**, **5**) exhibit electrocatalytic waves at substantially less negative potentials of −1.64, −1.62, and −1.63 V, respectively. The higher activities observed for **2**, **4**, and **5** photochemically are thus attributed to more facile reduction by Fl^{-}, leading to higher rates for hydrogen production (See Table 1).

Electrochemical Experiments in Water. In order to study the electrocatalytic activities of these complexes in aqueous media, several sets of experiments were performed. Cyclic voltammograms were obtained in a pH 7.0 aqueous phosphate buffer solutions using a glassy carbon working electrode. A 0.1 mM solution of complex **5** showed an irreversible catalytic reduction wave with a current density (j) of 20 mA/cm^2 at an overpotential (applied potential − E(pH 7)) of −700 mV (Figure 7B). In this experiment, H_2 bubbles were observed from the tip of the electrode during CV experiments. Complexes **2** and **4** also exhibited irreversible catalytic waves but at potentials more negative relative to **5**

DOI: 10.1021/acscatal.5b00045
ACS Catal. 2015, 5, 1397−1406

under similar electrocatalytic conditions. In the case of complex **2**, a current density (j) of 15 mA/cm^2 was seen at an overpotential of −800 mV (Figure S16). In control experiments without any catalyst or with simple $Ni(NO_3)_2$ salt, negligible current densities were observed (Figure 7B). It is noteworthy that although complexes **2**, **4**, and **5** show similar catalytic proton reduction potentials in acetonitrile with added acetic acid, a difference is seen in potentials for the catalytic waves in 1.0 M pH 7 phosphate buffer. The Faradaic efficiencies (f) of **2** and **5** for electrocatalytic H_2 production were assessed using controlled potential coulometric experiments in pH 7 phosphate buffer at different overpotentials. The amount of H_2 generated from the headspace of the electrochemical cell was determined by gas chromatography. The Faradaic efficiency was then calculated by comparing the amount of H_2 with the total charge passed in the system. For catalyst **5**, f = 98 ± 5% was obtained in the range of −380 to −780 mV overpotential after a 1 h period, whereas f = 93 ± 5% (−480 to −880 mV overpotential) was found for catalyst **2**. Figures 8 and S17 (for complexes **5** and **2**, respectively) show that the rate of the electrocatalytic hydrogen production increases with increasing applied potential.

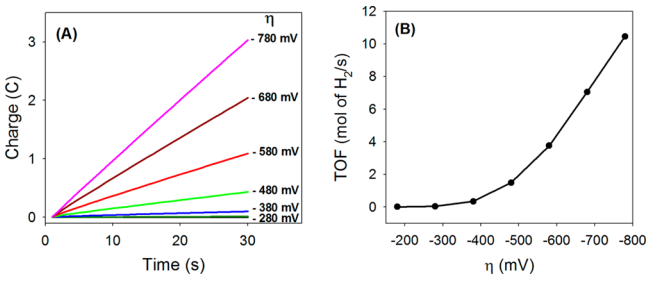

Figure 8. (A) Charge passed over time from electrolysis of a solution of **5** (10 μM, 5 mL) in 1.0 M phosphate buffer at pH 7.0 under Ar at various overpotentials. Glassy carbon as the working electrode and a platinum mesh as the counter electrode, Ag/AgCl (3.0 M KCl) as the reference electrode. Overpotential (η = applied potential − E (pH 7)). (B) TOF versus overpotential. TOF was calculated based on the total amount of **5** in solution.

Another criterion for the development of more practical catalysts for H_2 production is whether the catalyst is O_2 tolerant. Although [FeFe] hydrogenases in nature have very high reactivity for proton reduction, they are typically sensitive to ambient oxygen,[61] with only a few examples showing catalyst tolerance for O_2.[62−64] In order to study this aspect of catalytic behavior, both CV and controlled potential coulometric experiments were performed in air with complexes **2** and **5**. After CV experiments under argon (Figure 7B, S15), solutions were purged with air for 2 min, after which new CVs were measured. The latter CVs in air show no difference from the ones performed under Ar. Controlled potential coulometry experiments with solutions of **2** and **5** in pH 7.0 phosphate buffer in air give Faradaic efficiencies of 78 ± 3% and 80 ± 4%, respectively, after 1 h of electrolysis. A control experiment in air shows that the charge passed in the absence of catalyst is less than 7% of the amount generated by a 10 μM solution of **5** even at −750 mV overpotential (Figure S18). The decreased Faradaic efficiencies in the presence of air are presumably due to reduction of oxygen. To assess the robustness of the catalyst in air, long-term controlled potential coulometric experiments were performed in 2.0 M pH 7 phosphate buffers. Faradaic efficiencies close to 80% were determined at the beginning and at the end of the experiment, indicating that the catalyst is stable (i.e., its activity is maintained) during the entire period. A TON over 80 000 mol of H_2 per mole of catalyst for **5** and 62 000 mol of H_2 per mole of catalyst for **2** was achieved after 40 h of electrolysis based on the total charge passed (Figure S20−21). The constant rate for charge passed per unit time highlights the robustness of these catalysts operating in air (Figure S20−21).

The catalytic properties of complexes of **2** and **5** were also evaluated using different water sources that included water from the Genesee River containing significant particulate matter and seawater from the Gulf of Mexico. Both of these water samples were passed through paper filters and buffered at pH 7.0 by the addition of 1.0 M phosphate salts. As shown in Figure S22 and S23, the experiments using sea or river water gave no difference in rate during hydrogen production at a −580 mV overpotential over 30 min for **5** and −650 mV overpotential for **2**, as compared to the studies conducted in distilled water. Catalysts **2** and **5** thus appear robust even in the presence of dissolved impurities in river and seawater samples.

Chemical Reduction of Protons. We also made efforts to simplify study of the reduction by using chemical reductants in place of PS or electrode. The chemical interconversion of **2** and **6**, which is formally the product of hydrogen addition to **2**, is shown in Scheme 2. The reaction was monitored by UV−vis spectroscopy in both directions. Addition of 2 equiv acetic acid to a solution of **2** in DMF followed by the addition of 2 equiv of decamethylcobaltocene ($CoCp^*_2$) as reducing agent leads to **6** *without* any evidence of H_2 generation by GC analysis. Spectroscopic change is only seen upon the addition of $CoCp^*_2$, and isosbestic points are observed in UV−vis spectra, indicating that the only Ni-containing species are **2** and **6**, without any buildup of intermediates or Ni-containing byproducts with significant visible absorptions. In the reverse reaction, conversion of **6** to **2** by treatment with NEt_3 as base followed 2 equiv of ferrocenium tetrafluoroborate as oxidizing agent, solution color change and growth of the prominent LLCT band of **2** occur *only* upon addition of Fc^+.

Complex **6** exhibits the same catalytic activity for H_2 generation as **2** under photochemical conditions (Figure S24), suggestive of different entry points to the same catalytic cycle. However, **6** does not liberate H_2 upon heating and/or the addition of $CoCp^*_2$, meaning that it cannot be the intermediate directly preceding H_2 evolution. However, with the use of a stronger reducing agent (Na/Hg), **6** does lead to generation of $\mathbf{2}^-$ (Figure S25) and the observation of H_2 (Scheme 3) by GC analysis. Subsequent addition of 1 equiv of $[Cp_2Fe]BF_4$ to this system leads to immediate formation of **2**, as shown by its characteristic LLCT band at 825 nm. The LLCT band of $\mathbf{2}^-$ is at lower energy than that of **2** (Figure S25) and is similar in intensity to that of the isoelectronic complex $Ni(bdt)_2^-$, **1**, as shown in Figure 1. Based on these observations, it is reasonable to assign $\mathbf{6}^-$ as the intermediate directly preceding H_2 evolution which is common to both **2** and **6** upon irradiation, as described below.

For complex **5**, addition of 3 equiv of trifluoroacetic acid (TFA) to a DMSO solution of **5** does not show any change in the ^{1}H NMR spectrum (Figure S5 and S26). Instead, addition of 1 equiv of $CoCp^*_2$ to a solution of **5** results in an immediate color change from yellow to dark orange, and the appearance of paramagnetically shifted signals in the ^{1}H NMR spectrum (Figure S27). These observations are consistent with the

DOI: 10.1021/acscatal.5b00045
ACS Catal. 2015, 5, 1397−1406

Scheme 3. Proposed Pathway for the Formation of Hydrogen from 6 Consistent with ECEC Electrochemical Mechanism

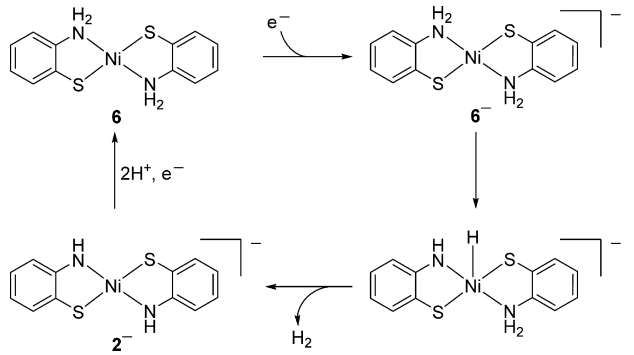

formation of a one-electron reduced species. Reduction of **5** thus appears to be the initial step in proton reduction and is consistent with the electrochemical data (see Figure 7A) showing noncatalytic reduction of Ni^{2+} to Ni^{+} that precedes the turnover limiting step of hydrogen formation.

To determine the possibility of $2e^-$ reduction of **5** to a Ni^0 species during catalysis, an analogous experiment was carried out using Na/Hg as a stronger reductant than $CoCp^*_2$. After the addition of an excess amount of Na/Hg to a dry DMSO solution of **5**, the solution color changes slowly to dark orange and then to green. Although isolation of these intermediates was not successful, the first color change (from yellow to dark orange) monitored by ^1H NMR spectroscopy corresponds to generation of the same species observed when using $CoCp^*_2$ as the reductant. The diamagnetic signals in the ^1H NMR spectrum of the green species suggest the formation of a Ni^0 species (Figure S28). This green species turns orange upon exposure to air, which may correspond to formation of the Ni^+ species described above. However, the green solution shows only three aromatic ^1H NMR signals instead of four expected from the mpo ligand, indicating the possibility of **5** undergoing ligand decomposition when reduced beyond the Ni^+ state. It is important to note that the CV of **5** shows no observable Ni^+/Ni^0 wave at values less negative than −2 V (vs SCE), suggesting that two consecutive reductions to form such a highly reduced species is thermodynamically unfavorable and therefore unlikely to occur in the pathway for proton reduction.

After addition of one equivalent of TFA to the dark orange species generated by $CoCp^*_2$ reduction of **5**, the color of the solution changed to light orange. There was no hydrogen detected by GC at this step. However, when another equivalent of $CoCp^*_2$ was added to the solution, gas bubbles were observed and confirmed to be H_2 by GC analysis. Continued additions of TFA and $CoCp^*_2$ successively resulted in H_2 generation but only after the addition of $CoCp^*_2$ reductant. Although the studies described in this section were conducted in organic solvents, the results give insight into the mechanism for H_2 formation by **2** and **5** in aqueous/organic media.

Mechanism for Proton Reduction and H_2 Formation. For H_2 formation, two e^- and two H^+ must be collected and assembled prior to product elimination. In the catalytic cycle, the turnover limiting step represents the highest kinetic barrier in the cycle and controls the rate at which the overall catalysis proceeds. The fact that the electrocatalytic waves for the most active catalysts (**5** and **2**) are at potentials more negative than seen in the absence of acid suggests that the turnover limiting step in the catalysis involves the second reduction in the H_2 forming cycle. The notion of reduction as the turnover limiting step is supported by the chemical investigations in which H_2 is formed upon the addition of chemical reductant such as $CoCp^*_2$.

The mechanism of H_2 formation thus involves initial reduction of the catalyst followed by protonation. For **2**, the initial site of reduction is likely to be ligand-based based on literature precedent for the redox activity of aminothiophenolate in nickel complexes,[55,56] whereas for **5**, the more negative potential indicates that the mpo ligand is not redox active, and the reduction site is likely to be the metal ion. On the basis of the computational results for the related catalyst $[Co(bdt)_2]^-$,[45] the initial protonation site for **2** is also proposed to be ligand-based. Overall, this suggests an ECEC mechanism for electrocatalysis of proton reduction using **2**, where the second, turnover-limiting reduction is followed by the second protonation and a heterocoupling step involving a ligand-bound proton and a metal-bound hydride. In the case of **5**, whereas mpo is not considered to be a redox active ligand, it is possible that the *N*-oxide donor may serve as a protonation site for delivery of H^+ to a Ni-bound hydride.

The generation of H_2 from $\mathbf{6}^-$ is consistent with these proposals for H_2 formation. Specifically, following the reductions and ligand protonations of **2** to form **6**, further reduction to $\mathbf{6}^-$ facilitates a proton shift to give a metal hydride species that can react with a ligand-bound proton to form H_2 (Scheme 3). This heterocoupling ($H^- + H^+ \rightarrow H_2$) is well-precedented in hydrogenase model complexes,[65] as well as Ni pyridylthiolate and pyrimidinethiolate catalysts.[18,39]

CONCLUSION

A series of square planar nickel complexes have been studied as catalysts for the light-driven reduction of protons to H_2, and several have been found to be highly active using either Fl or CdSe QDs as the photosensitizer. The active light-driven H_2 production systems function in water and exhibit notable durability as well as overall photochemical stability. The catalysts can function under a wide pH range that depends on the particular sacrificial donor employed. Electrochemical studies of these catalysts have also been performed and reveal higher activities of **2**, **4**, and **5** relative to the other two complexes. Bulk electrolysis with **2** and **5** in neutral pH water gives almost quantitative Faradaic yields, even with impure and/or salty water, indicating notable robustness. In the case of **2**, ligand-centered reductions occur upon the addition of chemical reducing agent followed by protonation of the ligands in the presence of weak acid, whereas in the case of **5**, preferential metal-centered reduction occurs. Both chemical and electrochemical studies strongly suggest that the active Ni catalysts described here follow an ECEC mechanism for the formation of hydrogen even though the initial sites of reduction differ.

EXPERIMENTAL SECTION

Materials. All starting materials were purchased from Aldrich unless mentioned otherwise. All solvents were used without further purification unless otherwise stated. Sea water was purchased from Aldrich. Genesee River water was obtained directly during a summer month. Pentaerythritol tribromide was purchased from AK Scientific Ltd. and used without further purification. The syntheses of CdSe-TOPO (TOPO =

DOI: 10.1021/acscatal.5b00045
ACS Catal. 2015, 5, 1397−1406

trioctylphosphine oxide), CdSe-DHLA (DHLA = dihydrolipoic acid), and CdSe-S3 were accomplished according to the literature procedures.[20,47]

*Preparation of (^{n}Bu$_4$N)[Ni(bdt)$_2$] (**1**).* Complex **1** was synthesized following a literature reported procedure.[48] Under N_2, 92 mg (4 mmol) of Na was dissolved in 25 mL of absolute ethanol, to which 284 mg (2 mmol) of benzene-1,2-dithiol was then added. Addition of a solution of $NiCl_2.6H_2O$ (235 mg, 1 mmol) in 5 mL ethanol resulted in the formation of a reddish brown precipitate, after which 320 mg (1 mmol) of ^{n}Bu$_4$NBr was added, and the mixture was stirred initially under N_2 for 30 min and then under air for 24 h. The color of the mixture gradually turned to dark green. The precipitate was collected by filtration and washed with cold absolute ethanol. The crude product was recrystallized from dichloromethane/ether to yield dark green crystals of **1** (350 mg, 69%). Elem. Anal. Calcd: C, 57.82; H, 7.63; N, 2.41. Found: C, 57.91; H, 7.53; N, 2.29. ^{1}H NMR DMSO-d_6: 3.13 (bs), 1.55 (bs), 1.29 (bs), 0.92 (bs) (no distinct signals are observed for the aromatic protons).

*Preparation of [Ni(abt)$_2$] (**2**).* The procedure was adopted from the literature method.[53] 2-Aminothiophenol (500 mg, 4 mmol) and potassium hydroxide (220 mg, 4 mmol) were dissolved in 10 mL of 20% aqueous ethanol. To this solution, a solution of $NiCl_2{\cdot}6H_2O$ (470 mg, 2 mmol) in 10 mL of 2.5 M aqueous ammonia was added dropwise with stirring. A yellow colored precipitate was formed immediately. The solution was stirred for 30 min, and then the precipitate was collected by filtration. The precipitate was suspended in 30 mL of water containing 400 mg of potassium hydroxide, and air was bubbled through the solution for 6 h, resulting in the formation of dark blue precipitate. The precipitate was collected by filtration and crystallized from diethyl ether to give dark blue microcrystals of compound **2** (410 mg, 67%). Elem. Anal. Calcd: C, 47.25; H, 3.30; N, 9.18. Found: C, 47.38; H, 3.36; N, 8.95. ^{1}H NMR CD_2Cl_2: 9.15 (bs, 2H), 7.82 (d, 2H), 7.38 (d, 2H), 7.24 (t, 2H), 7.15 (t, 2H).

*Preparation of [Ni(pda)$_2$] (**3**).* This procedure was adapted from the literature method.[52] Five hundred milligrams (2.1 mmol) of $NiCl_2{\cdot}6H_2O$ was dissolved in 5 mL of 8.0 M aqueous ammonia solution. This solution was added to a solution of 460 mg (4.2 mmol) of *o*-phenylenediamine in 40 mL of warm water (50 °C). The mixture was stirred in air for 24 h. A dark blue precipitate was collected by filtration and purified by methods reported in the literature.[52] Yield was 330 mg (58%, based on isolated crystalline product). Elem. Anal. Calcd: C, 53.19; H, 4.46; N, 20.68. Found: C, 52.96; H, 4.47; N, 20.36. ^{1}H NMR DMSO-d_6: 8.85 (s, 4H), 7.01 (dd, 4H), 6.71 (dd, 4H).

*Preparation of (^{n}Bu$_4$N)[Ni(mp)$_2$] (**4**).* The procedure was adapted from a reported literature method.[53] To a 30 mL 7:3 (v/v) EtOH/H_2O solution containing 1.0 g (8 mmol) of *o*-mercaptophenol and 0.65 g (8 mmol) of sodium hydroxide was added dropwise a solution of 30 mL of 7:3 (v/v) EtOH/H_2O solution containing $Ni(NO_3)_2{\cdot}6H_2O$ (1.15 g, 4 mmol). After the resultant solution turned dark brown, 1.67 g (5 mmol) of Bu_4NBr in 8 mL of EtOH was added. After passing air through the solution for 1 h, the crude product was collected by filtration. Long green needle crystals could be obtained from 1:3 (v/v) acetone/toluene at −20 °C (15% yield). A unit cell of the crystal was determined by X-ray diffraction and found to match the reported structure. Elem. Anal. Calcd: C, 61.2; H, 8.07; N, 2.55. Found: C, 59.76; H, 7.75; N, 2.58. ^{1}H NMR DMSO- d_6: 3.20 (bs), 1.62 (bs), 1.36 (bs), 0.98 (bs) (no distinct signals are observed for the aromatic protons).

*Preparation of [Ni(mpo)$_2$] (**5**).* The procedure was taken from the reported method.[53] $NiCl_2{\cdot}6H_2O$ (0.96g, 4 mmol) was dissolved in 150 mL of 3:5 (v/v) MeOH/MeCN mixture, to which was added 2.0 equiv of Na(mpo) (1.2 g, 8.0 mmol) as solid. The mixture was allowed to stir in air overnight. After filtration, the crude product was collected by evaporating the filtrate under vacuum. Large brown block crystals were obtained from acetone by slow evaporation at room temperature (85% yield). A unit cell of the crystal was determined by X-ray diffraction and found to match the reported structure. Elem. Anal. Calcd: C, 38.62; H, 2.59; N, 9.01. Found: C, 38.52; H, 2.56; N, 8.83. ^{1}H NMR DMSO- d_6: 8.74 (d, 2H), 7.59 (d, 2H), 7.415 (t, 2H), 7.155 (t, 2H).

Light-Driven Hydrogen Evolution Studies. Samples were prepared in 40 mL scintillation vials and protected from light prior to use. The total volume of the solution was 5.0 mL, with the pH adjusted by the addition of HCl or NaOH. The samples were placed into a temperature-controlled block at 15 °C and sealed with an airtight cap fitted with a pressure transducer and a rubber septum. The samples were then degassed with a mixture of gas containing 4:1 N_2/CH_4. The methane present in the gas mixture serves as an internal reference for GC analysis at the end of the experiment. The cells were irradiated from below the vials with high power Philips LumiLED Luxeon Star Hex green (520 nm) 700 mA LEDs. The light power of each LED was set to 130 mW and measured at the top of the cell with an L30 A Thermal sensor and Nova II power meter (Ophir-Spiricon LLC). The samples were swirled using an orbital shaker. The pressure changes in the vials were recorded using a Labview program from a Freescale semiconductor sensor (MPX4250A series). At the end of the experiment, the headspace of each vial was characterized by gas chromatography to ensure that the measured pressure change was caused solely by hydrogen generation and to double check that the amount of generated hydrogen calculated by the change in pressure corresponded to the amount determined by the GC analysis. The amounts of hydrogen evolved were determined with a Shimadzu GC-17A gas chromatograph with a 5 Å molecular sieve column (30 m, 0.53 mm) and a TCD detector by injection of 100 μL samples of headspace gas, and the amounts were quantified by a calibration plot to the internal CH_4 standard.

Spectroscopic Studies. UV−vis-NIR spectra of the complexes were recorded on a Cary 60 UV−vis spectrophotometer in their corresponding DMF solutions. The concentration of the samples was 10^{-5} M. For UV−vis studies during photolysis with Fl as PS, aliquots of 30 μL of the photolysis solutions were collected by syringe at different time periods, diluted by a factor of 100 in distilled water and measured on the Cary 60 UV/vis spectrophotometer. For UV−vis studies for the interconversion of **2** and **6**, a 1×10^{-5} M solution of each complex was prepared in dry DMF and then 2.0 equiv of acetic acid (for **2**) or triethylamine (for **6**) was added first followed by addition of 2.0 equiv of $Co(Cp^*)_2$ (for **2**) or $FcBF_4$ (for **6**). ^{1}H NMR spectra were recorded on a Bruker Avance 400 MHz spectrometer and are reported in ppm at room temperature. All spectra were referenced to the residual solvent peak.

Cyclic Voltammetry. Cyclic Voltammetry (CV) measurements of the catalyst were performed with a CHI 680D potentiostat using a one-compartment cell with a glassy carbon working electrode, glassy carbon auxiliary electrode (3.0 mm in

DOI: 10.1021/acscatal.5b00045
ACS Catal. 2015, 5, 1397−1406

diameter), and SCE reference electrode. The electrolyte for electrochemistry in MeCN/DMF was 0.1 M tetrabutylammonium hexafluorophosphate ($TBAPF_6$) and the electrolyte in H_2O was 1.0 M pH 7.0 phosphate buffer. Argon was used to purge all samples if not specified. In the acid concentration dependence study, a 2.0 M stock solution of acetic acid was prepared in MeCN/DMF with 0.1 M $TBAPF_6$. To a stirred and degassed solution of 0.5 mM catalyst, 5−10 μL of acid stock solution was added, and the mixture was purged with argon for another 300 s before performing cyclic voltammetry.

Controlled-Potential Coulometry. A custom-built air-tight three-chambered electrochemical cell was used. All three electrodes were placed in separate chambers containing a 1.0 to 3.0 M pH 7.0 phosphate buffer solution. The chamber holding the working electrode also contains 10 μM to 40 μM of catalysts. Fine-porosity glass frits were used to separate each chamber. Glassy carbon disks (3.0 mm in diameter) or cylinders of reticulated vitreous carbon (0.5 cm in radius and 1.0 cm in height) were used as the working electrode. A platinum mesh was used as the auxiliary electrode. The reference electrode was a Ag/AgCl (3.0 M KCl) electrode. The cell was purged with a mixture of gas containing 4:1 N_2/CH_4 for 15 min. The methane present in the gas mixture serves as an internal reference for GC analysis. For the 1 h experiments, the amount of H_2 produced was quantified from an analysis of the headspace of the chamber containing the working electrode using the same method as the light-driven hydrogen production experiments. Faradaic efficiencies were determined by dividing the measured H_2 produced by the amount of H_2 expected on the basis of charge passed during the controlled-potential electrolysis measurments.

In the longer controlled potential electrolysis experiments, gas evolution led to solution level differences between cell chambers. Consequently, for longer duration experiments (44 h), the amount of H_2 evolved and Faradaic efficiencies were determined *only* in the first and the last 1 h periods to verify that the catalyst is stable through the entire period of irradiation. At other times, the H_2 generated was vented to maintain equal pressure in all chambers.

Overpotential Determination. Overpotentials were calculated using the following equation: overpotential = applied potential − E(pH), where E(pH) = (−0.059 × pH) V. CV experiments were done using SCE as the reference electrode and controlled potential coulometry experiments were performed using Ag/AgCl (3.0 M KCl) as the reference electrode. Applied potential (vs SHE) were obtained by adding 0.244 V (for SCE) or 0.210 V (for Ag/AgCl (3.0 M KCl)) with the experimentally obtained potential values.

Photolysis with Added Mercury. The sample was prepared following the same procedure as described above for the regular photolysis experiment. A 5 mL solution of 2 mM fluorescein was prepared in 5% TEOA with 20 μM of **2**. The pH of the solution was adjusted to 9.8, after which ∼1 mL of liquid Hg was introduced before degassing. Another photocatalytic solution was prepared with the same concentrations of all components but without added Hg. The amount of H_2 produced was monitored by the change of pressure and quantified by GC analysis at the end of photocatalysis.

X-ray Diffraction Studies. Crystals were placed onto the tips of glass capillary tubes or fibers and mounted on a Bruker SMART CCD platform diffractometer for data collection. For each crystal, a preliminary set of cell constants and an orientation matrix were calculated from reflections harvested from three orthogonal wedges of reciprocal space. Full data collections were carried out using Mo Kα radiation (0.71073 Å, graphite monochromator) with frame time of 60 s and at a detector distance of approximately 4 cm. Randomly oriented regions of reciprocal space were surveyed: three to six major sections of frames were collected with 0.50° steps in ω at four and six φ settings and a detector position of −38° in 2θ. The intensity data were corrected for absorption.[66] Final cell constants were calculated from the xyz centroids of a few thousand strong reflections from the actual data collections after integration.[67]

Structures were solved using SIR2011[68] and refined using SHELXL-2013.[69] Space groups were determined on the basis of systematic absences, intensity statistics, or both. Direct-methods solutions were calculated, which provided most non-hydrogen atoms from the E map. Full-matrix least-squares/difference Fourier cycles were performed which located the remaining non-hydrogen atoms. All non-hydrogen atoms were refined with anisotropic displacement parameters. All hydrogen atoms were placed in ideal positions and refined as riding atoms with relative isotropic displacement parameters. Full-matrix least-squares refinements on F^2 were run to convergence.

■ ASSOCIATED CONTENT

Supporting Information

The following files are available free of charge on the ACS Publications website at DOI: 10.1021/acscatal.5b00045.

NMR data, electrochemistry data, and control photocatalysis data (PDF)

X-ray crystallographic data (CIF)

■ AUTHOR INFORMATION

Corresponding Author

*E-mail: eisenberg@chem.rochester.edu.

Author Contributions

#A.D. and Z.H. contributed equally to this work.

Notes

The authors declare no competing financial interest.

■ ACKNOWLEDGMENTS

We wish to thank the Division of Chemical Sciences, Geosciences, and Biosciences, Office of Basic Energy Sciences, U.S. Department of Energy, Grant DE-FG02-09ER16121 for support of the research involving the use of QD photosensitizers, and the National Science Foundation (CHE-1151789) for support of research involving the use of organic dyes as photosensitizers.

■ REFERENCES

(1) U.S. Department of Energy, Energy Information Administration, Annual Energy Outlook 2013 with Projections to 2040. U.S. Government Printing Office: Washington, DC, 2013; pp55−90.

(2) U. S. Department of Energy, Energy Information Administration, International Energy Outlook 2013 with Projections to 2040. U.S. Government Printing Office: Washington, DC, 2013; pp 1−22.

(3) Hoffert, M. I.; Caldeira, K.; Jain, A. K.; Haites, E. F.; Harvey, L. D. D.; Potter, S. D.; Schlesinger, M. E.; Schneider, S. H.; Watts, R. G.; Wigley, T. M. L.; Wuebbles, D. J. *Nature* **1998**, *395*, 881.

(4) Alstrum-Acevedo, J. H.; Brennaman, M. K.; Meyer, T. J. *Inorg. Chem.* **2005**, *44*, 6802.

(5) Lewis, N. S.; Nocera, D. G. *Proc. Natl. Acad. Sci. U.S.A.* **2006**, *103*, 15729.

(6) Bard, A. J.; Fox, M. A. *Acc. Chem. Res.* **1995**, *28*, 141.

DOI: 10.1021/acscatal.5b00045
ACS Catal. 2015, 5, 1397−1406

(7) Streich, D.; Astuti, Y.; Orlandi, M.; Schwartz, L.; Lomoth, R.; Hammarstrøm, L.; Ott, S. *Chem.—Eur. J.* **2010**, *16*, 60.
(8) White, T. A.; Whitaker, B. N.; Brewer, K. J. *J. Am. Chem. Soc.* **2011**, *133*, 15332.
(9) DiSalle, B. F.; Bernhard, S. *J. Am. Chem. Soc.* **2011**, *133*, 11819.
(10) Singh, W. M.; Baine, T.; Kudo, S.; Tian, S. L.; Ma, X. A. N.; Zhou, H. Y.; DeYonker, N. J.; Pham, T. C.; Bollinger, J. C.; Baker, D. L.; Yan, B.; Webster, C. E.; Zhao, X. *Angew. Chem., Int. Ed.* **2012**, *51*, 5941.
(11) McCrory, C. C. L.; Uyeda, C.; Peters, J. C. *J. Am. Chem. Soc.* **2012**, *134*, 3164.
(12) Helm, M. L.; Stewart, M. P.; Bullock, R. M.; Rakowski DuBois, M.; DuBois, D. L. *Science* **2011**, *333*, 863.
(13) Marinescu, S. C.; Winkler, J. R.; Gray, H. B. *Proc. Natl. Acad. Sci. U.S.A.* **2012**, *109*, 15127.
(14) Zhang, P. L.; Wang, M.; Gloaguen, F.; Chen, L.; Quentelb, F.; Sun, L. C. *Chem. Commun.* **2013**, *49*, 9455.
(15) Du, P. W.; Eisenberg, R. *Energy Environ. Sci.* **2012**, *5*, 6012.
(16) Kagalwala, H. N.; Gottlieb, E.; Li, G.; Li, T.; Jin, R. C.; Bernhard, S. *Inorg. Chem.* **2013**, *52*, 9094.
(17) McNamara, W. R.; Han, Z. J.; Yin, C. J.; Brennessel, W. W.; Holland, P. L.; Eisenberg, R. *Proc. Natl. Acad. Sci. U.S.A.* **2012**, *109*, 15594.
(18) Han, Z.; Shen, L.; Brennessel, W. W.; Holland, P. L.; Eisenberg, R. *J. Am. Chem. Soc.* **2013**, *135*, 14659.
(19) Luo, S. P.; Mejia, E.; Friedrich, A.; Pazidis, A.; Junge, H.; Surkus, A. E.; Jackstell, R.; Denurra, S.; Gladiali, S.; Lochbrunner, S.; Beller, M. *Angew. Chem., Int. Ed.* **2013**, *52*, 419.
(20) Han, Z.; Qiu, F.; Eisenberg, R.; Holland, P. L.; Krauss, T. D. *Science* **2012**, *338*, 1321.
(21) Eckenhoff, W. T.; McNamara, W. R.; Du, P.; Eisenberg, R. *Biochim. Biophys. Acta, Bioenerg.* **2013**, *1827*, 958.
(22) Artero, V.; Chavarot-Kerlidou, M.; Fontecave, M. *Angew. Chem., Int. Ed.* **2011**, *50*, 7238.
(23) Du, P. W.; Knowles, K.; Eisenberg, R. *J. Am. Chem. Soc.* **2008**, *130*, 12576.
(24) Fihri, A.; Artero, V.; Razavet, M.; Baffert, C.; Leibl, W.; Fontecave, M. *Angew. Chem., Int. Ed.* **2008**, *47*, 564.
(25) Probst, B.; Rodenberg, A.; Guttentag, M.; Hamm, P.; Alberto, R. *Inorg. Chem.* **2010**, *49*, 6453.
(26) Lazarides, T.; McCormick, T.; Du, P. W.; Luo, G. G.; Lindley, B.; Eisenberg, R. *J. Am. Chem. Soc.* **2009**, *131*, 9192.
(27) McCormick, T. M.; Calitree, B. D.; Orchard, A.; Kraut, N. D.; Bright, F. V.; Detty, M. R.; Eisenberg, R. *J. Am. Chem. Soc.* **2010**, *132*, 15480.
(28) Hawecker, J.; Lehn, J. M.; Ziessel, R. *Nouv. J. Chim.* **1983**, *7*, 271.
(29) McCormick, T. M.; Han, Z. J.; Weinberg, D. J.; Brennessel, W. W.; Holland, P. L.; Eisenberg, R. *Inorg. Chem.* **2011**, *50*, 10660.
(30) Simándi, L. I.; Szeverényi, Z.; Budó-Záhonyi, É. *Inorg. Nucl. Chem. Lett.* **1975**, *11*, 773.
(31) Karunadasa, H. I.; Chang, C. J.; Long, J. R. *Nature* **2010**, *464*, 1329.
(32) Karunadasa, H. I.; Montalvo, E.; Sun, Y. J.; Majda, M.; Long, J. R.; Chang, C. J. *Science* **2012**, *335*, 698.
(33) Sun, Y.; Bigi, J. P.; Piro, N. A.; Tang, M. L.; Long, J. R.; Chang, C. J. *J. Am. Chem. Soc.* **2011**, *133*, 9212.
(34) Nippe, M.; Khnayzer, R. S.; Panetier, J. A.; Zee, D. Z.; Olaiya, B. S.; Head-Gordon, M.; Chang, C. J.; Castellano, F. N.; Long, J. R. *Chem. Sci.* **2013**, *4*, 3934.
(35) Stewart, M. P.; Ho, M. H.; Wiese, S.; Lindstrom, M. L.; Thogerson, C. E.; Raugei, S.; Bullock, R. M.; Helm, M. L. *J. Am. Chem. Soc.* **2013**, *135*, 6033.
(36) Hoffert, W. A.; Roberts, J. A. S.; Bullock, R. M.; Helm, M. L. *Chem. Commun.* **2013**, *49*, 7767.
(37) McLaughlin, M. P.; McCormick, T. M.; Eisenberg, R.; Holland, P. L. *Chem. Commun.* **2011**, *47*, 7989.
(38) Silver, Sunshine C.; Pingwu Du, J. N.; Poluektov, Oleg G.; Tiede, David M.; Utschig, Lisa M. *J. Am. Chem. Soc.* **2013**, *135*, 13246.
(39) Han, Z. J.; McNamara, W. R.; Eum, M. S.; Holland, P. L.; Eisenberg, R. *Angew. Chem., Int. Ed.* **2012**, *51*, 1667.
(40) Han, Z.; Eisenberg, R. *Acc. Chem. Res.* **2014**, *47*, 2537.
(41) Eisenberg, R.; Gray, H. B. *Inorg. Chem.* **2011**, *50*, 9741.
(42) Eisenberg, R. *Coord. Chem. Rev.* **2011**, *255*, 825.
(43) Sproules, S.; Wieghardt, K. *Coord. Chem. Rev.* **2011**, *255*, 837.
(44) Lyaskovskyy, V.; de Bruin, B. *ACS Catal.* **2012**, *2*, 270.
(45) Solis, B. H.; Hammes-Schiffer, S. *J. Am. Chem. Soc.* **2012**, *134*, 15253.
(46) McNamara, W. R.; Han, Z.; Alperin, P. J.; Brennessel, W. W.; Holland, P. L.; Eisenberg, R. *J. Am. Chem. Soc.* **2011**, *133*, 15368.
(47) Das, A.; Han, Z. J.; Haghighi, M. G.; Eisenberg, R. *Proc. Natl. Acad. Sci. U.S.A.* **2013**, *110*, 16716.
(48) Baker-Hawkes, M.-J.; Billig, E.; Gray, H. B. *J. Am. Chem. Soc.* **1966**, *88*, 4870.
(49) Balch, A. L. *J. Am. Chem. Soc.* **1969**, *91*, 1948.
(50) Robinson, M. A. *J. Inorg. Nucl. Chem.* **1964**, *26*, 1277.
(51) Chen, X. T.; Hu, Y. H.; Wu, D. X.; Weng, L. H.; Kang, B. S. *Polyhedron* **1991**, *10*, 2651.
(52) Balch, A. L.; Holm, R. H. *J. Am. Chem. Soc.* **1966**, *88*, 5201.
(53) Holm, R. H.; Balch, A. L.; Davison, A.; Maki, A. H.; Berry, T. E. *J. Am. Chem. Soc.* **1967**, *89*, 2866.
(54) Xie, J.-L.; Ren, X.-M.; He, C.; Song, Y.; Duan, C.-Y.; Gao, S.; Meng, Q.-J. *Polyhedron* **2003**, *22*, 299.
(55) Herebian, D.; Bothe, E.; Bill, E.; Weyhermüller, T.; Wieghardt, K. *J. Am. Chem. Soc.* **2001**, *123*, 10012.
(56) Bachler, V.; Olbrich, G.; Neese, F.; Wieghardt, K. *Inorg. Chem.* **2002**, *41*, 4179.
(57) Köckerling, M.; Henkel, G. *Chem. Ber.* **1993**, *126*, 951.
(58) Ji-Cheng, S.; Ting-Bin, W.; Yu, Z.; Shin-Jun, Z.; Da-Xu, W.; Qiu-Tian, L.; Bei-Sheng, K.; Bo-Mu, W.; Mak, T. C. W. *Polyhedron* **1997**, *16*, 369.
(59) Xiong, R.-G.; Song, B.-L.; You, X.-Z.; Mak, T. C. W.; Zhou, Z.-Y. *Polyhedron* **1996**, *15*, 991.
(60) Bhattacharya, S.; Gupta, P.; Basuli, F.; Pierpont, C. G. *Inorg. Chem.* **2002**, *41*, 5810.
(61) Fontecilla-Camps, J. C.; Volbeda, A.; Cavazza, C.; Nicolet, Y. *Chem. Rev.* **2007**, *107*, 5411.
(62) Mondal, B.; Sengupta, K.; Rana, A.; Mahammed, A.; Botoshansky, M.; Dey, S. G.; Gross, Z.; Dey, A. *Inorg. Chem.* **2013**, *52*, 3381.
(63) Sit, P. H. L.; Car, R.; Cohen, M. H.; Selloni, A. *Proc. Natl. Acad. Sci. U.S.A.* **2013**, *110*, 2017.
(64) Kleingardner, J. G.; Kandemir, B.; Bren, K. L. *J. Am. Chem. Soc.* **2013**, *136*, 4.
(65) Carroll, M. E.; Barton, B. E.; Rauchfuss, T. B.; Carroll, P. J. *J. Am. Chem. Soc.* **2012**, *134*, 18843.
(66) Sheldrick, G. M. *SADABS*, version 2012/1; University of Göttingen: Göttingen, Germany, 2012.
(67) *SAINT*, version 8.27B; Bruker AXS: Madison, WI, 2013.
(68) Burla, M. C.; CaliandroR.Camalli, M.; Carrozzini, B.; Cascarano, G. L.; Giacovazzo, C.; Mallamo, M.; Mazzone, A.; Polidori, G.; Spagna, R. *SIR2011: a new package for crystal structure determination and refinement*, version 1.0; Istituto di Cristallografia: Bari, Italy, 2012.
(69) Sheldrick, G. M. *SHELXL-2013/4*; University of Göttingen: Göttingen, Germany, 2013.

DOI: 10.1021/acscatal.5b00045
ACS Catal. 2015, 5, 1397−1406